

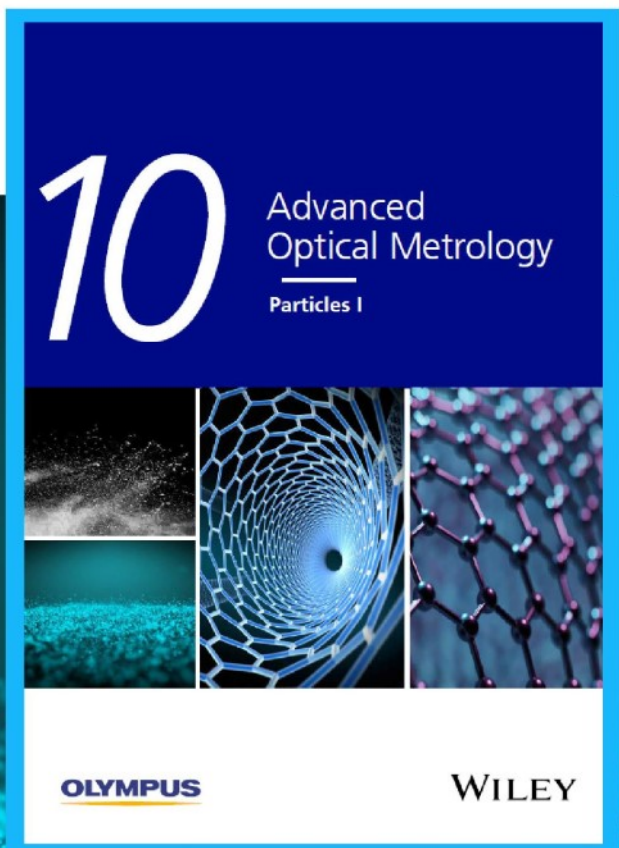


Particles I

Access the latest eBook →

Particles: Unique Properties,
Uncountable Applications

**Read the latest eBook and
better your knowledge with
highlights from the recent
studies on the design and
characterization of micro-
and nanoparticles for
different application areas.**



Access Now

This eBook is sponsored by

OLYMPUS

WILEY

Polarization-Driven-Orientation Selective Growth of Single-Crystalline III-Nitride Semiconductors on Arbitrary Substrates

Danshuo Liu, Lin Hu, Xuelin Yang,* Zhihong Zhang, Haodong Yu, Fawei Zheng, Yuxia Feng, Jiaqi Wei, Zidong Cai, Zhenghao Chen, Cheng Ma, Fujun Xu, Xinqiang Wang, Weikun Ge, Kaihui Liu, Bing Huang,* and Bo Shen*


III-nitride semiconductor films are usually achieved by epitaxial growth on single-crystalline substrates (sapphire, silicon (Si), and silicon carbide). It is important to grow these films on non-epitaxial substrates of interest such as polycrystalline substrates for exploring novel applications in electronics and optoelectronics. However, single-crystalline III-nitride films with uniform orientation on non-epitaxial substrates have not yet been realized, due to the lack of crystallographic orientation of the substrates. Here, this work proposes a strategy of polarization-driven-orientation selective growth (OSG) and demonstrate that single-crystalline gallium nitride (GaN) can in principle be achieved on any substrates. Taking polycrystalline diamond and amorphous-silicon dioxide/Si substrates as typical examples, the OSG is demonstrated by utilizing a composed buffer layer consisting of graphene and polycrystalline physical vapor deposited (PVD) aluminium nitride (AlN). The polarization of the PVD AlN can effectively tune the strength of interfacial orbital coupling between AlN nuclei and graphene at different rotation angles, as confirmed by atom-scale first-principles calculations, and align the AlN nuclei to form a uniform orientation. This consequently leads to continuous single-crystalline GaN films. The ability to grow single-crystalline III-nitrides onto any desired substrates would create unprecedented opportunities for developing novel electronic and optoelectronic devices.

1. Introduction

For semiconductor films, the mainstream of their growth methods relies on epitaxy including homogeneous as well as heterogeneous epitaxy.^[1-7] There is a golden rule that both epitaxial approaches require single-crystalline substrates for deposition. For instance, III-nitride semiconductors have a wide range of modern applications,^[3,8-11] representing an extremely important semiconductor family today, for which the present commonly adopted substrates for their epitaxial growth are single-crystalline sapphire, silicon carbide, silicon (Si), and gallium nitride (GaN).^[3,9,12,13] In order to explore novel applications in next-generation electronics and optoelectronics,^[10,11] it is highly demanded to grow single-crystalline GaN films on non-epitaxial substrates of interest such as polycrystalline diamond substrates, amorphous glass substrates, and fused silica substrates. However, even after decades of intensive attempts, it

D. S. Liu, X. L. Yang, Z. H. Zhang, J. Q. Wei, Z. D. Cai, Z. H. Chen, C. Ma, F. J. Xu, X. Q. Wang, W. K. Ge, K. H. Liu, B. Shen
State Key Laboratory of Artificial Microstructure and Mesoscopic Physics
Nano-optoelectronics Frontier Center of Ministry of Education
School of Physics
Peking University
Beijing 100871, P. R. China
E-mail: xlyang@pku.edu.cn; bshen@pku.edu.cn
L. Hu, B. Huang
Beijing Computational Science Research Center
Beijing 100193, P. R. China
E-mail: bing.huang@csr.ac.cn

L. Hu, F. W. Zheng
Centre for Quantum Physics
Key Laboratory of Advanced Optoelectronic Quantum Architecture
and Measurement (MOE)
School of Physics
Beijing Institute of Technology
Beijing 100081, P. R. China
X. L. Yang, X. Q. Wang, B. Shen
Peking University Yangtze Delta Institute of Optoelectronics
Nantong 226010, P. R. China
H. D. Yu
School of Physical Science and Technology & Key Laboratory
for Magnetism and Magnetic Materials of the MOE
Lanzhou University
Lanzhou 730000, P. R. China

 The ORCID identification number(s) for the author(s) of this article can be found under <https://doi.org/10.1002/adfm.202113211>.

DOI: 10.1002/adfm.202113211

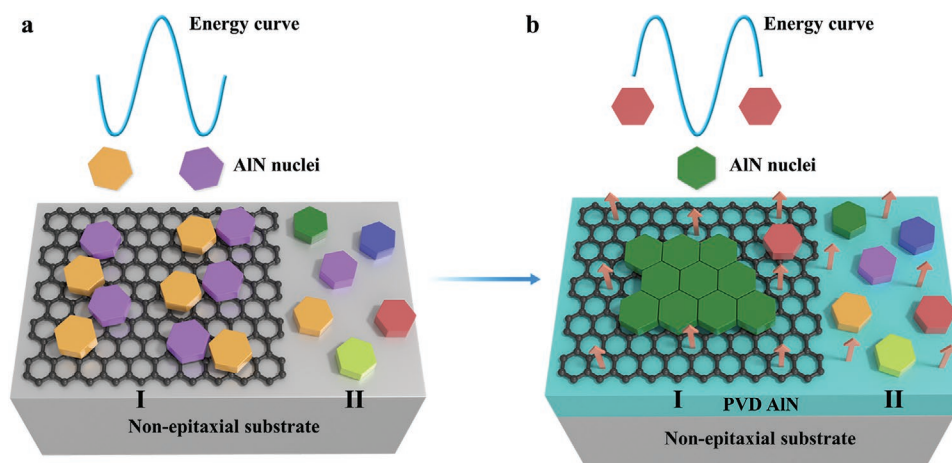


Figure 1. Schematic diagram of conventional growth and polarization-driven-orientation selective growth of AlN nuclei on graphene. a) Conventional strategy of growth of AlN nuclei on graphene (a, region I) leads to dual in-plane orientations with $\approx 30^\circ$ misalignment. b) OSG of AlN nuclei on graphene/PVD AlN (b, region I) leads to single in-plane orientation of AlN nuclei, which also benefits to the subsequent coalescence growth. AlN nuclei directly grown on either non-epitaxial substrates (a, region II) or PVD AlN (b, region II) without graphene leads to random in-plane orientations. Different colors of AlN nuclei indicate different rotation angles. Top curves represent the energy curve for each orientation. Arrows represent the existence of polarization field.

remains a fundamental challenge to achieve single-crystalline GaN on non-single-crystalline substrates due to the absence of crystallographic orientation of these substrates. Although the nearly single-crystalline GaN, in the form of either pyramid arrays or strip shape, has been obtained on amorphous glass substrates^[14] and silicon dioxide (SiO_2)/Si templates^[15] via local growth in a confined area, it is not surprising that the continuous single-crystalline GaN films with uniform orientation on non-epitaxial substrates still cannot be realized.

It is rational to speculate that the marriage of single-crystalline GaN and such substrates may require a 2D buffer layer, for example, graphene,^[16,17] as a bridge, which can provide the hexagonal symmetry and guide the growth of wurtzite GaN. In fact, several pioneering studies have demonstrated the possibility of growth of single-crystalline GaN on graphene, either by van der Waals epitaxy^[18–25] or remote epitaxy.^[26–29] However, most of the substrates underlying the graphene are still limited to be single crystalline. In addition, the physics behind the growth mechanism is still controversial.^[16,24,26,30] Very recent work reported the growth of GaN on amorphous silica glass substrates using nanorod-assisted van der Waals epitaxy.^[31] However, the obtained GaN exhibit three in-plane orientations, far deviating from single-crystalline. Thus, whether the graphene can be used as a buffer for growth of single-crystalline

GaN films on a non-epitaxial substrate remains an open question. The answer to this question is not only of great significance from the view point of fundamental physics, but also will hopefully open up new opportunities for integration of GaN films with arbitrary substrates and thus for a large range of industrial applications. How to precisely control the in-plane orientation of GaN on graphene and finally select a stable in-plane orientation is the main obstacle to be overcome.

The basic idea is to tune the energy curve of the system at different in-plane orientation configurations via an external field. It is known that the polarization can shift the orbital energy levels, giving rise to their most favorable orbital coupling at different configurations and eventually selecting a new ground energy state.^[32,33] Here, we introduce a polarization-driven-orientation selective growth (OSG) strategy to achieve single-crystalline GaN films with uniform orientation on arbitrary substrates. By employing a composed buffer layer of single-crystalline graphene and polycrystalline physical vapor deposited (PVD) aluminium nitride (AlN), the polarization of the PVD AlN may effectively shift the relative interfacial orbital positions between AlN nuclei and graphene, giving rise to the most favorable selective orbital coupling at different in-plane rotation angles. Consequently, the energy curve of the system at different angles can be effectively tuned, for example, the initial low (high) energy configurations may become to the high (low) energy one, which may eventually stabilize a single-preferred orientation.

2. Results and Discussion

A schematic diagram of the strategy is shown in **Figure 1**. Generally, the AlN nuclei directly grown on non-epitaxial substrates would exhibit random in-plane orientations (Figure 1 (a, region II), Figure 1 (b, region II), and **Figure 2a**). By employing a hexagonal graphene alone, the in-plane orientation of the AlN nuclei can be limited to two dominant configurations

Y. X. Feng
Key Laboratory of Optoelectronics Technology
College of Microelectronics
Beijing University of Technology
Ministry of Education
Beijing 100124, P. R. China

X. Q. Wang, B. Shen
Collaborative Innovation Center of Quantum Matter
Beijing 100871, P. R. China

B. Huang
Department of Physics
Beijing Normal University
Beijing 100875, P. R. China

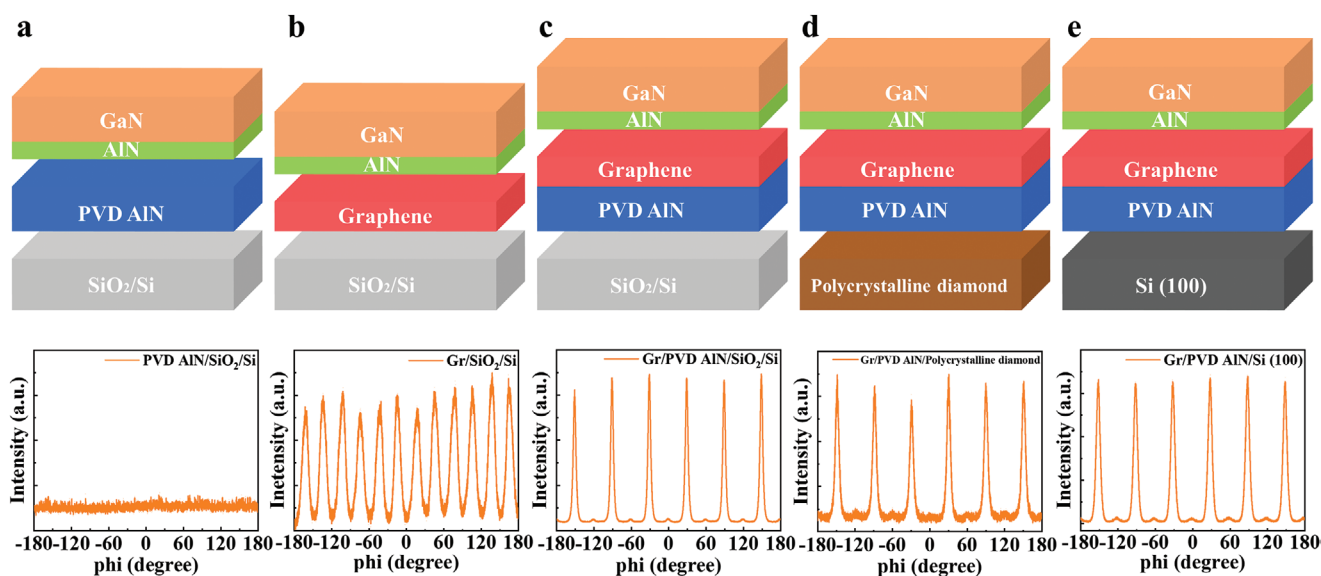


Figure 2. In-plane orientation of GaN grown on different types of substrates, characterized by XRD azimuthal off-axis ϕ scan on GaN (103) reflection. a) GaN grown on SiO_2/Si substrate with a PVD AlN buffer. Absence of any peaks in the ϕ scan indicates random in-plane orientations. b) GaN grown on SiO_2/Si substrate with a graphene buffer. Twelve peaks in the ϕ scan indicate dual in-plane orientations with 30° misalignment. GaN grown on an c) amorphous SiO_2/Si substrate, d) polycrystalline diamond substrate, and e) Si (100) substrate with a composed buffer of graphene/PVD AlN. All of the three samples exhibit sixfold symmetry, corresponding to a uniform in-plane alignment.

with $\approx 30^\circ$ misalignment (Figure 1 (a, region I) and Figure 2b). That is attributed to the two sets of energy-minimized configurations (whose orientation differs by 30°) with almost degenerate energies for AlN nuclei on pristine graphene due to the higher symmetry of graphene.^[21] By further inserting a PVD AlN layer underneath the graphene (Figure 1b), the energy curve is dramatically modified in the presence of the polarization of the PVD AlN, which selectively stabilizes a single-preferred in-plane orientation of AlN nuclei and hence accelerates the subsequent coalescence growth of single-crystalline AlN and GaN.

To experimentally verify whether the graphene/PVD AlN composed buffer can indeed achieve single-crystalline GaN growth with a uniform in-plane orientation, we performed the idea of OSG on three types of substrates, for example, amorphous SiO_2/Si substrates, polycrystalline diamond substrates, and Si (100) substrates, respectively. The PVD AlN typically exhibits polycrystalline characters with random in-plane orientations but uniform out-of-plane orientation (c -axis) (Figure S1, Supporting Information). The single-crystalline graphene was grown by chemical vapor deposition (CVD) method and then transferred to the PVD AlN surface.^[34] The graphene shows a high-quality monolayer property (Figure S2, Supporting Information).^[35] The graphene/PVD AlN templates were then loaded to a metal-organic chemical vapor deposition (MOCVD) reactor for the growth of AlN nuclei and GaN. The orientations of GaN on different substrates were investigated by X-ray diffraction (XRD) ϕ scan on the GaN (103) reflection. For all of the GaN samples grown on these three substrates, we can find six pronounced peaks with intensity maxima at intervals of 60° from the ϕ scan (Figure 2c–e), which clearly reveals the hexagonal structure of the grown layer and highlights the uniform in-plane alignment of the GaN grown on these substrates. That is in contrast to the randomly in-plane orientated GaN grown on

the substrates with either PVD AlN (Figure 2a and Figure S3a, Supporting Information) or graphene interlayer alone as the buffer layer (Figure 2b and Figure S3b, Supporting Information). These results imply the excellent orientation selective effect of the composed buffer of graphene/PVD AlN. The XRD 2θ scan further shows that the out-of-plane orientation of the GaN layer is fully aligned with the c -axis (Figure S4, Supporting Information).

We also conducted some controlled experiments, for example, changing the single-crystalline graphene to polycrystalline graphene. The XRD ϕ scan (Figure S5a, Supporting Information) then shows 12 unremarkable peaks with intensity maxima at intervals of 30° , indicating the coexistence of two configurations with 30° in-plane misorientation for the GaN films growth on the composed buffer layer of polycrystalline graphene/PVD AlN. It seems that the orientation of GaN solely comes from the single-crystalline graphene, and is not related to the underlying PVD AlN because of its polycrystalline nature. However, we emphasize that, without the PVD AlN, the pristine graphene itself cannot serve as an ideal buffer layer for single-crystalline GaN growth (Figures S3b and S5b, Supporting Information). It implies that single-crystalline graphene, together with PVD AlN, jointly play the key role of aligning the crystallographic orientation of the top AlN nuclei and GaN layer. In practice, the growth kinetics of the AlN nuclei should be carefully controlled to achieve single-crystalline GaN. For example, the conditions of high growth temperature ($\geq 1090^\circ\text{C}$) and low growth rate (trimethylaluminum (TMAI) flow rate ≤ 6 sccm) are required to provide sufficient energy (or time) for the AlN nuclei to rotate to the most favorable orientation on graphene, completing the unidirectional growth, as seen in Figure S6, Supporting Information.

To further understand the kinetics of the OSG of AlN nuclei on graphene/PVD AlN, we used scanning electron

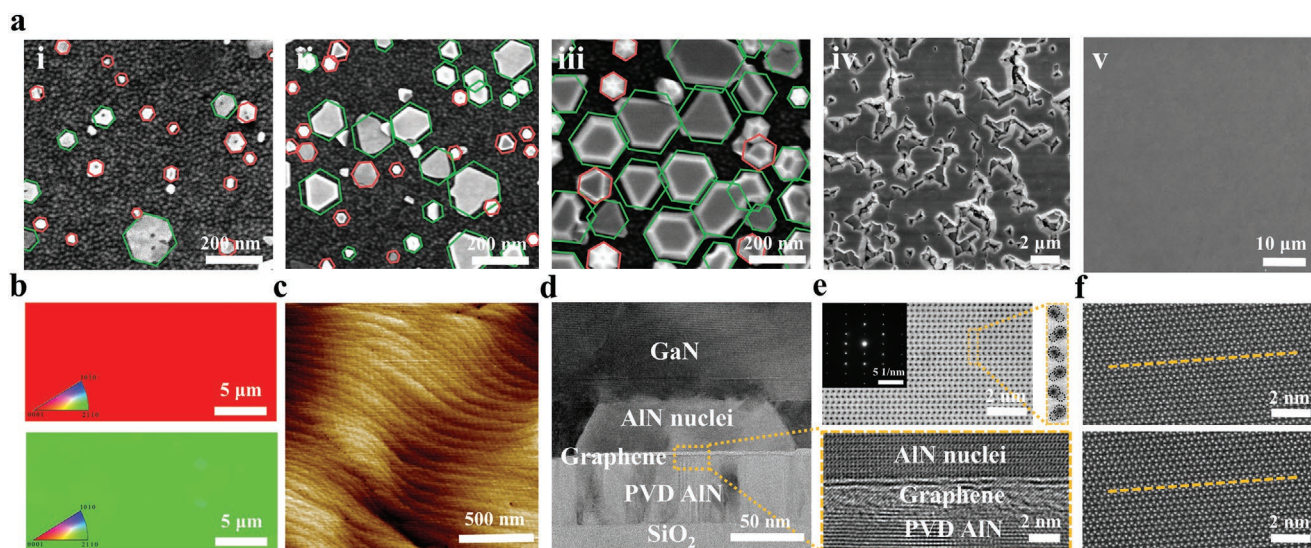


Figure 3. Surface morphologies and atomic structures of AlN nuclei and GaN on graphene/PVD AlN buffer. a) SEM images of (i to iii) AlN nuclei and (iv and v) GaN at different growth stages. There are mainly two kinds of AlN islands, that is, larger sized ones marked with green hexagonal lines, while smaller sized ones are marked with red lines. As the growth proceeds, the larger AlN nuclei are aligned along one direction, while the smaller ones are rotated 30° from that direction. Finally, a single-preferred in-plane orientation of AlN nuclei is formed. Subsequent coalescence growth of (iv) GaN leads to a continuous and flat single-crystalline (v) GaN film. b) Out-of-plane and in-plane EBSD maps showing the single crystallinity of the GaN film. c) AFM image of the GaN film, showing a step-flow surface morphology with a RMS of 0.35 nm. d) Cross-sectional HRTEM image taken at the interface region in the GaN/AlN/graphene/PVD AlN. Magnified image reveals the monolayer graphene in the sample. e) ABF-STEM image of GaN shows a clear wurtzite lattice structure. Ga and N atoms can be clearly identified from the magnified image. Inset: SAED pattern indicates the single crystallinity of the GaN layer. f) Representative atomically resolved STEM images indicate the uniform in-plane orientation of GaN.

microscopy (SEM) to investigate the evolution of the surface morphology of the AlN nuclei and GaN layer. From the SEM images (Figures 3ai–iii), we can find that there are mainly two kinds of AlN islands, that is, larger sized ones marked with green hexagonal lines, while smaller sized ones marked with red lines. Interestingly, as the growth proceeds, the larger AlN nuclei are aligned along one direction, while the smaller ones are rotated 30° from that direction. These results suggest that when the AlN nuclei reaches a critical size with increasing growth time, almost all the AlN nuclei are aligned along the same direction, that is, a single-preferred in-plane orientation of AlN nuclei is selected. Subsequent coalescence growth of GaN (Figure 3aiv) leads to a continuous single-crystalline GaN film uniformly covering the entire substrate surface (Figure 3av). The typical in situ reflectance curve (LayTec EpiCurve TT) (Figure S7, Supporting Information, the points A–E corresponding to the growth stage of Figures 3ai–v here, respectively) reveals that the growth mode transforms from 3D growth to 2D growth, and the final saturation of the oscillation amplitude also confirms a smooth surface of the GaN layer. The in situ reflectance curve is very similar to the case of epitaxial growth of GaN on single-crystalline substrates such as sapphire substrate.^[36]

We find that, by employing the PVD AlN underlayer, the density of the AlN nuclei on graphene is significantly enhanced (Figure S8a,c, Supporting Information), which also benefits to the sequent coalescence growth of the GaN layer (Figure S8b,d, Supporting Information). The Raman spectra and X-ray photoelectron spectroscopy (XPS) results (Figure S9, Supporting Information) confirm that the nucleation mechanism is fundamentally different from the general case where the nucleation of nitrides

is triggered by defects and wrinkles of graphene.^[18–23] The results here indicate that there exists a new nucleation mechanism for AlN on graphene/PVD AlN. By performing a first-principles density functional theory (DFT) calculation (Figure S10, Supporting Information), the enhanced nucleation is found to be attributed to the higher binding energy of AlN on graphene/PVD AlN.

The single crystallinity of the GaN layer was also confirmed by electron backscatter diffraction (EBSD) mappings (Figure 3b). A single color in the out-of-plane EBSD maps of the GaN film indicates that there is no azimuthal intermixing of the *c*-axis orientation while a single color in the in-plane EBSD maps indicates no azimuthal intermixing of the in-plane orientation in the GaN film either. The corresponding atomic force microscopy (AFM) image shows a smooth surface with atomic-step terraces (Figure 3c). The root mean square (RMS) roughness of the GaN film is as low as 0.35 nm. Although the surface is smooth, we have to note that the GaN still contains a large dislocation density, as estimated from the full-width at half-maximum (FWHM) value ($\approx 0.59^\circ$) of GaN (002) XRD rocking curves (Figure S11, Supporting Information). This value is larger than that for GaN grown on single-crystalline substrates, as expected, and can be reduced by further optimizing the growth conditions.

The atomic structures of the single-crystalline GaN film and AlN nuclei on graphene/PVD AlN were analyzed by cross-sectional high-resolution transmission electron microscopy (HRTEM) (Figure 3d). The magnified image indicates a perfect sharp interface between the AlN nuclei and graphene. The atomically resolved annular bright-field scanning transmission electron microscopy (ABF-STEM) image (Figure 3e) of the GaN shows a clear wurtzite lattice structure. The Ga and N atoms

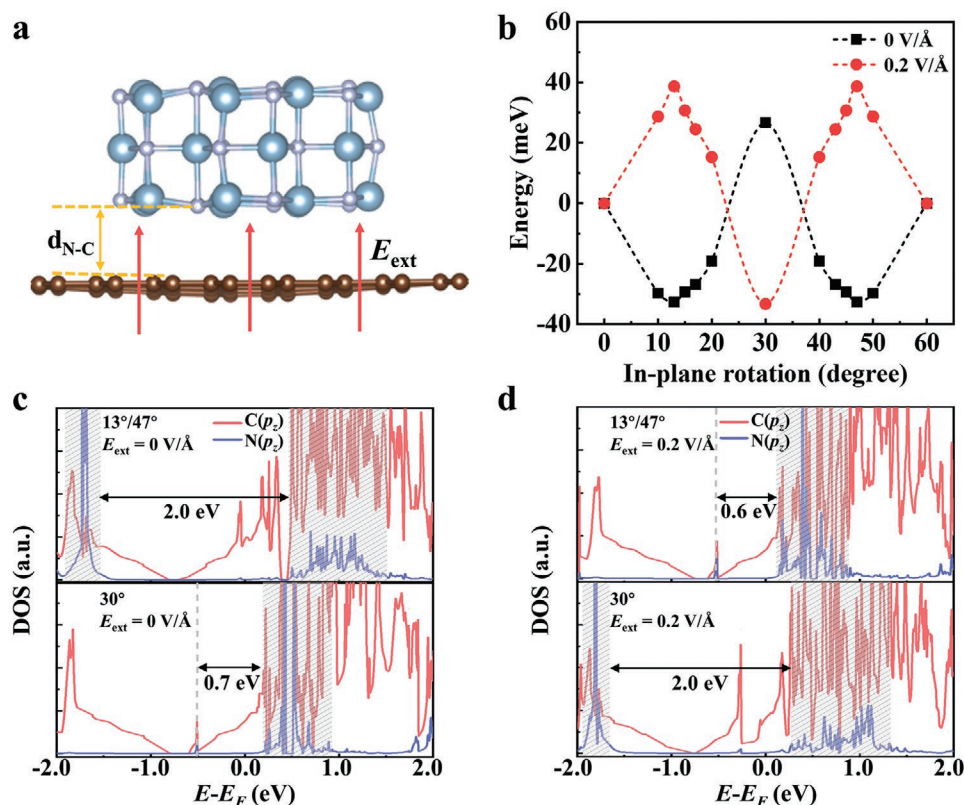


Figure 4. Mechanism of OSG of single-crystalline AlN on graphene. a) Side view of the model of 3×3 AlN nuclei on 10×10 graphene (3×3 AlN/ 10×10 graphene). The direction of the external electric field E_{ext} induced by PVD AlN is shown. b) Total energy changes of 3×3 AlN/ 10×10 graphene as a function of the in-plane rotation angles under $E_{\text{ext}} = 0$ and 0.2 V \AA^{-1} , respectively. When E_{ext} is turned on, the ground state is shifted from the double-degenerated $13^\circ/47^\circ$ configuration to the singlet 30° one. c, d) Comparison of partial density of states (PDOS) of interfacial N and C orbitals in 3×3 AlN/ 10×10 graphene at 13° (or 47°) and 30° under c) $E_{\text{ext}} = 0 \text{ V \AA}^{-1}$ and d) $E_{\text{ext}} = 0.2 \text{ V \AA}^{-1}$. The PDOS reveals the band repulsion effect (indicated by the black arrows) between interfacial orbitals has a dramatic change under E_{ext} , which is much stronger at $13^\circ/47^\circ$ (30°) configurations than that at 30° ($13^\circ/47^\circ$) configuration under $E_{\text{ext}} = 0$ (0.2) V \AA^{-1} .

can be clearly identified from the magnified image. The orientations of the GaN layers are also well aligned, as evidenced by the selected area electron diffraction pattern (SAED) in the inset in Figure 3e, which indicates the single crystallinity of the GaN layer. The atomically resolved STEM images at different positions confirm that the crystalline lattice of the GaN is indeed aligned along the same direction, as demonstrated in Figure 3f and Figure S12, Supporting Information. All these reveal that, by using the graphene/PVD AlN buffer, OSG of single-crystalline GaN can successfully be achieved on any free-standing substrates, breaking the widely believed golden rule.

As we mentioned above, the PVD AlN exhibits polycrystalline behaviors containing lots of small grains with a uniform c -axis orientation whereas random in-plane orientations (Figure S1, Supporting Information). This structure is non-centrosymmetric while it has a singular polar axis causing the formation of strong polarization and ensuing an electrical field along c -axis.^[3,37,38] As schematically shown in Figure 1, comparing the case without the PVD AlN buffer layer, the polarization induced E_{ext} may effectively shift the relative energy levels between the interfacial N p and C p orbitals, giving rise to their most favorable orbital coupling at a different angle. To verify this physical picture, we have investigated the total energy

and electronic structure evolutions of 3×3 AlN/ 10×10 graphene with different in-plane rotation angles from 0° to 60° (Figure 4a,b). Without E_{ext} , there exist two ground-state configurations at 13° and 47° with the same minimal total energy that agreed well with the existence of a minimum $d_{\text{N-C}}$ at these angles (Figure S13a, Supporting Information). The 34° misorientation is consistent with our experimental observation for the direct growth of AlN on graphene (Figure 2b and Figures S3b and S5b, Supporting Information). Interestingly, when E_{ext} is turned on, the ground state is shifted from the double-degenerated $13^\circ/47^\circ$ configuration to the singlet 30° one, also consisting well with a single minimum $d_{\text{N-C}}$ at 30° configuration (Figure S13a, Supporting Information). The energy differences between the 30° configuration and other configurations are obvious and will increase as the E_{ext} increases (Figure S13b, Supporting Information) and also as the size of the AlN nuclei increases (Figure S13c, Supporting Information). This indicates that the AlN nuclei will favor to rotate to the 30° configuration to lower their total energies when they become larger. That is well consistent with the SEM images (Figures 3ai–iii).

In order to further understand the electronic structure evolution corresponding to the ground-state configuration changes under E_{ext} , we have plotted the partial density of states (PDOS),

focusing on the selective coupling between interfacial N and C orbitals. The N p_z and C p_z orbitals around the Fermi level can have symmetry-allowed band repulsion, forming a separation of the bonding-like and antibonding-like hybridized N p_z -C p_z states in energy. Generally, the larger the band repulsion, the larger the energy gain of the system, and consequently, the lower the total energy of the system. As shown in Figure 4c, when $E_{\text{ext}} = 0 \text{ V \AA}^{-1}$, the more delocalized bonding-like and antibonding-like states (shadowed area) are formed at $13^\circ/47^\circ$ configurations, and the band repulsion effect is much stronger than that at 30° configuration. This is also consistent with the observation of the minimum total energy (or $d_{\text{N-C}}$, Figure S13a, Supporting Information) at $13^\circ/47^\circ$. Oppositely, when $E_{\text{ext}} = 0.2 \text{ V \AA}^{-1}$, as shown in Figure 4d, the band repulsion effect at 30° is much stronger than that at $13^\circ/47^\circ$ configurations and other configurations (such as that at $0^\circ/60^\circ$ configurations, Figure S14, Supporting Information), which effectively shifts the ground state from $13^\circ/47^\circ$ to 30° . Again, this is consistent with the minimum total energy (or $d_{\text{N-C}}$, Figure S13a, Supporting Information) occurring at the 30° configuration under $E_{\text{ext}} = 0.2 \text{ V \AA}^{-1}$. The calculations, together with experimental results, indicate the polarization effect induced by the PVD AlN is the key to achieving single-crystalline GaN growth. In fact, for the case of single-crystalline substrates, the polarity can modulate the atomic interaction through 2D material and lead to van der Waals epitaxy or remote epitaxy.^[26,27] Obviously, further investigations are required to correlate the present growth mechanism with either van der Waals epitaxy or remote epitaxy.

3. Conclusion

In conclusion, we have proposed an OSG strategy and demonstrated that it can be adopted to achieve single-crystalline semiconductor films on arbitrary non-epitaxial freestanding substrates, a long-awaited goal for decades. Single-crystalline GaN was chosen for the demonstration of the idea of the OSG. The OSG was enabled by a composed buffer layer of single-crystalline graphene and PVD AlN. The polarization of the PVD AlN can effectively tune the most favorable rotation angles for interfacial orbital coupling between AlN nuclei and graphene, realizing the transition from double-preferred to single-preferred orientation. It is an excellent example of orientation control mechanism in crystal growth based on the outstanding agreement between the calculations and experimental data. Such OSG approach provides unprecedented opportunities for integration of III-nitrides onto arbitrary freestanding substrates, for example, polycrystalline or amorphous, in which any substrate symmetry is not required. It can also be extended to the growth of other emergent single-crystalline semiconductor films on arbitrary freestanding substrates by choosing appropriate 2D materials with matched crystal structures.

4. Experimental Section

PVD AlN Growth: The AlN was sputtered on the target substrates by PVD. The sputtering gas was an Ar/N₂ mixture, with flow rates of 30 and 180 sccm for Ar and N₂, respectively. The total sputtering chamber pressure

range was 4.3 mTorr. The sputtering temperature was 650 °C with an input DC power of 3000 W. The thickness of the PVD AlN was about 50 nm.

Graphene Growth and Transfer: High-quality single-crystalline graphene was grown on single-crystal Cu (111) substrate by CVD using CH₄ as precursors. The graphene was then transferred on the PVD AlN template substrates by a PMMA-mediated wet transfer method. Graphene film was spin-coated with PMMA and baked at 120 °C for 2 min, and then the Cu was removed by 4% (NH₄)₂S₂O₈ solution. Finally, the PMMA was removed by acetone. More details can be found in previous work.^[21] The polycrystalline graphene was grown on Cu (100) substrate and directly transferred onto PVD AlN template. The polycrystalline graphene mainly contained two orientations with about 30° misalignment.

MOCVD Growth of AlN and GaN: The AlN nuclei and GaN layers were grown by MOCVD system (Aixtron, close-coupled-showerhead). TMAI, trimethylgallium (TMGa), and ammonia (NH₃) were used as the precursors for aluminum, gallium, and nitrogen, respectively. After the graphene transfer, the substrates were loaded into the MOCVD reactor and heated to the growth temperature of AlN nuclei under a hydrogen ambient and a pressure of 100 mbar. Once the temperature was ramped to the growth temperature (970–1090 °C) of AlN nuclei, TMAI and NH₃ were simultaneously injected into the reactor and started the growth of AlN nuclei without any surface pretreatment of the substrates. The flow rate of TMAI and NH₃ were 6 and 22 sccm, respectively. After the growth of AlN nuclei for 10 min, the precursor was switched from TMAI to TMGa for the growth of GaN under the conventional growth conditions.^[21]

Computational Model: The DFT calculations were performed with the Vienna ab initio simulation package.^[39] The Perdew–Burke–Ernzerhof (PBE) exchange correlation functional was employed with the cutoff energy of 600 eV.^[40] The van der Waals corrections were included to obtain the accurate interlayer interaction.^[41] The criterion of energy and forces were set to 1×10^{-6} eV and 0.01 eV \AA^{-1} , respectively. The optimized lattice constants of AlN and graphene were $a = b = 3.13 \text{ \AA}$ and $a = b = 2.46 \text{ \AA}$, respectively. The vacuum in c-direction was set to 15 Å. The k-mesh of these simulations was chosen as a single Γ point for structural relaxation due to the extreme large supercell size. For the electronic calculations, a dense k-mesh of $7 \times 7 \times 1$ was set to get accurate DOSs.

Characterization: XRD experiments were performed with X'Pert³ MRD system. SEM images were acquired using a Helios NanoLab 600i system at an accelerating voltage of 10 kV. EBSD maps were obtained using a Zeiss Merlin system at an accelerating voltage of 20 kV and the sample stage tilting at 70°. STEM/HRTEM experiments were performed using Thermo Scientific Themis Z at 200 kV. AFM images were acquired in tapping mode over the scan area, using a Bruker Dimensional ICON system in ambient atmosphere. Raman spectra were obtained with Horiba iHR550 system with a laser excitation wavelength of 488 nm about 5 mW power. XPS spectra were obtained using an AXIS Supra system. OM experiments were performed with OLYMPUS BX60M system and the images were acquired by a 3.0M Pixel CCD system.

Supporting Information

Supporting Information is available from the Wiley Online Library or from the author.

Acknowledgements

This work was supported by the National Natural Science Foundation of China (Nos. 61922001, 61927806, and 12088101), the National Key Research and Development Program of China (Nos. 2021YFB3600901 and 2018YFE0125700), and the Key Research and Development Program of Guangdong Province (Nos. 2019B010128002 and 2020B010171002), and NSAF (No. U1930402). Part of the computations was performed at Tianhe2-JK at CSRC.

Conflict of Interest

The authors declare no conflict of interest.

Data Availability Statement

The data that support the findings of this study are available from the corresponding author upon reasonable request.

Keywords

arbitrary substrates, in-plane orientation, polarization-driven-orientation selective growth, physical vapor deposited AlN, single-crystalline GaN, single-crystalline graphene

Received: December 24, 2021

Revised: January 25, 2022

Published online: February 11, 2022

- [1] R. Yan, G. Khalsa, S. Vishwanath, Y. Han, J. Wright, S. Rouvimov, D. S. Katzer, N. Nepal, B. P. Downey, D. A. Muller, H. G. Xing, D. J. Meyer, D. Jena, *Nature* **2018**, 555, 183.
- [2] Y. Chen, Y. Lei, Y. Li, Y. Yu, J. Cai, M.-H. Chiu, R. Rao, Y. Gu, C. Wang, W. Choi, H. Hu, C. Wang, Y. Li, J. Song, J. Zhang, B. Qi, M. Lin, Z. Zhang, A. E. Islam, B. Maruyama, S. Dayeh, L.-J. Li, K. Yang, Y.-H. Lo, S. Xu, *Nature* **2020**, 577, 209.
- [3] P. Waltereit, O. Brandt, A. Trampert, H. T. Grahn, J. Menniger, M. Ramsteiner, M. Reiche, K. H. Ploog, *Nature* **2000**, 406, 865.
- [4] Y. Kobayashi, K. Kumakura, T. Akasaka, T. Makimoto, *Nature* **2012**, 484, 223.
- [5] T.-A. Chen, C.-P. Chuu, C.-C. Tseng, C.-K. Wen, H.-S. P. Wong, S. Pan, R. Li, T.-A. Chueh, Y. Zhang, Q. Fu, B. I. Yakobson, W.-H. Chang, L.-J. Li, *Nature* **2020**, 579, 219.
- [6] M. Yoshimoto, K. Yoshida, H. Maruta, Y. Hishitani, H. Koinuma, S. Nishio, M. Kakihana, T. Tachibana, *Nature* **1999**, 399, 340.
- [7] M. V. Kelso, N. K. Mahenderkar, Q. Chen, J. Z. Tubbesing, J. A. Switzer, *Science* **2019**, 364, 166.
- [8] Z. Zheng, L. Zhang, W. Song, S. Feng, H. Xu, J. Sun, S. Yang, T. Chen, J. Wei, K. J. Chen, *Nat. Electron.* **2021**, 4, 595.
- [9] Y. Sun, K. Zhou, Q. Sun, J. Liu, M. Feng, Z. Li, Y. Zhou, L. Zhang, D. Li, S. Zhang, M. Ikeda, S. Liu, H. Yang, *Nat. Photon* **2016**, 10, 595.
- [10] H. Amano, Y. Baines, E. Beam, M. Borga, T. Bouchet, P. R. Chalker, M. Charles, K. J. Chen, N. Chowdhury, R. Chu, C. D. Santi, M. M. D. Souza, S. Decoutere, L. D. Cioccio, B. Eckardt, T. Egawa, P. Fay, J. J. Freedman, L. Guido, O. Haberlen, G. Haynes, T. Heckel, D. Hemakumara, P. Houston, J. Hu, M. Hua, Q. Huang, A. Huang, S. Jiang, H. Kawai, et al., *J. Phys. D: Appl. Phys.* **2018**, 51, 163001.
- [11] M. Kneissl, T.-Y. Seong, J. Han, H. Amano, *Nat. Photon* **2019**, 13, 233.
- [12] T. Hashimoto, F. Wu, J. S. Speck, S. Nakamura, *Nat. Mater.* **2007**, 6, 568.
- [13] Z. Yan, G. Liu, J. M. Khan, A. A. Balandin, *Nat. Commun.* **2012**, 3, 827.
- [14] J. H. Choi, A. Zoulkarneev, S. I. Kim, C. W. Baik, M. H. Yang, S. S. Park, H. Suh, U. J. Kim, H. B. Son, J. S. Lee, M. Kim, J. M. Kim, K. Kim, *Nat. Photon* **2011**, 5, 763.
- [15] B. Leung, J. Song, Y. Zhang, J. Han, *Adv. Mater.* **2013**, 25, 1285.
- [16] S.-H. Bae, H. Kum, W. Kong, Y. Kim, C. Choi, B. Lee, P. Lin, Y. Park, J. Kim, *Nat. Mater.* **2019**, 18, 550.
- [17] J. Yu, L. Wang, Z. Hao, Y. Luo, C. Sun, J. Wang, Y. Han, B. Xiong, H. Li, *Adv. Mater.* **2020**, 32, 1903407.
- [18] J. Kim, C. Bayram, H. Park, C.-W. Cheng, C. Dimitrakopoulos, J. A. Ott, K. B. Reuter, S. W. Bedell, D. K. Sadana, *Nat. Commun.* **2014**, 5, 4836.
- [19] K. Qiao, Y. Liu, C. Kim, R. J. Molnar, T. Osadchy, W. Li, X. Sun, H. Li, R. L. Myers-Ward, D. Lee, S. Subramanian, H. Kim, K. Lu, J. A. Robinson, W. Kong, J. Kim, *Nano Lett.* **2021**, 9, 4013.
- [20] Z. Chen, X. Zhang, Z. Dou, T. Wei, Z. Liu, Y. Qi, H. Ci, Y. Wang, Y. Li, H. Chang, J. Yan, S. Yang, Y. Zhang, J. Wang, P. Gao, J. Li, Z. Liu, *Adv. Mater.* **2018**, 30, 1801608.
- [21] Y. Feng, X. Yang, Z. Zhang, D. Kang, J. Zhang, K. Liu, X. Li, J. Shen, F. Liu, T. Wang, P. Ji, F. Xu, N. Tang, T. Yu, X. Wang, D. Yu, W. Ge, B. Shen, *Adv. Funct. Mater.* **2019**, 29, 1905056.
- [22] F. Liu, Z. Zhang, X. Rong, Y. Yu, T. Wang, B. Sheng, J. Wei, S. Zhou, X. Yang, F. Xu, Z. Qin, Y. Zhang, K. Liu, B. Shen, X. Wang, *Adv. Funct. Mater.* **2020**, 30, 2001283.
- [23] D. Liang, T. Wei, J. Wang, J. Li, *Nano Energy* **2020**, 69, 104463.
- [24] S. Shervin, M. Moradnia, M. K. Alam, T. Tong, M.-H. Ji, J. Chen, S. Pouladi, T. Detchprohm, R. Forrest, J. Bao, R. D. Dupuis, J.-H. Ryou, *J. Mater. Chem. C* **2021**, 9, 2243.
- [25] J. W. Shon, J. Ohta, K. Ueno, A. Kobayashi, H. Fujioka, *Sci. Rep.* **2014**, 4, 5325.
- [26] Y. Kim, S. S. Cruz, K. Lee, B. O. Alawode, C. Choi, Y. Song, J. M. Johnson, C. Heidelberger, W. Kong, S. Choi, K. Qiao, I. Almansouri, E. A. Fitzgerald, J. Kong, A. M. Kolpak, J. Hwang, J. Kim, *Nature* **2017**, 544, 340.
- [27] W. Kong, H. Li, K. Qiao, Y. Kim, K. Lee, Y. Nie, D. Lee, T. Osadchy, R. J. Molnar, D. K. Gaskill, R. L. M. Ward, K. M. Daniels, Y. Zhang, S. Sundram, Y. Yu, S. H. Bae, S. Rajan, Y. S. Horn, K. Cho, A. Ougazzaden, J. C. Grossman, J. Kim, *Nat. Mater.* **2018**, 17, 999.
- [28] T. Journot, H. Okuno, N. Mollard, A. Michon, R. Dagher, P. Gergaud, J. Dijon, A. V. Kolobov, B. Hyot, *Nanotechnology* **2019**, 30, 505603.
- [29] K. Badokas, A. Kadys, J. Mickevicius, I. Ignatjev, M. Skapas, S. Stanionytė, E. Radiunas, G. Juška, T. Malinauskas, *J. Phys. D: Appl. Phys.* **2021**, 54, 205103.
- [30] D. Jang, C. Ahn, Y. Lee, S. Lee, H. Lee, D. Kim, Y.-K. Kwon, J. Choi, C. Kim, arXiv:2110.01429, v1, submitted: October **2021**.
- [31] F. Ren, B. Liu, Z. Chen, Y. Yin, J. Sun, S. Zhang, B. Jiang, B. Liu, Z. Liu, J. Wang, M. Liang, G. Yuan, J. Yan, T. Wei, X. Yi, J. Wang, Y. Zhang, J. Li, P. Gao, Z. Liu, Z. Liu, *Sci. Adv.* **2021**, 7, 5011.
- [32] B. Yang, B. Shao, J. Wang, Y. Li, C. Y. Yam, S. Zhang, B. Huang, *Phys. Rev. B* **2021**, 103, L201405.
- [33] S. R. Wagner, B. Huang, C. Park, J. Feng, M. Yoon, P. Zhang, *Phys. Rev. Lett.* **2015**, 115, 096101.
- [34] H. Wang, T. Maiyalagan, X. Wang, *ACS Catal.* **2012**, 2, 781.
- [35] A. C. Ferrari, J. C. Meyer, V. Scardaci, C. Casiraghi, M. Lazzeri, F. Mauri, S. Piscanec, D. Jiang, K. S. Novoselov, S. Roth, A. K. Geim, *Phys. Rev. Lett.* **2006**, 97, 187401.
- [36] S. Figge, T. Böttcher, S. Einfeldt, D. Hommel, *J. Cryst. Growth* **2000**, 221, 262.
- [37] F. Bernardini, V. Fiorentini, *Phys. Rev. B* **1997**, 56, R10024.
- [38] O. Ambacher, J. Smart, J. R. Shealy, N. G. Weimann, K. Chu, M. Murphy, W. J. Schaff, L. F. Eastman, R. Dimitrov, L. Wittmer, M. Stutzmann, W. Rieger, J. Hilsenbeck, *J. Appl. Phys.* **1999**, 85, 3222.
- [39] G. Kresse, J. Hafner, *Phys. Rev. B* **1994**, 49, 14251.
- [40] J. P. Perdew, K. Burke, M. Ernzerhof, *Phys. Rev. Lett.* **1996**, 77, 3865.
- [41] S. Grimme, *J. Comput. Chem.* **2006**, 27, 1787.